7.4 Helium Effects in Advanced Structural Alloys: Progress on Solving a Grand Challenge to Fusion Energy — G. R. Odette, T. Yamamoto, Y. Wu, E. Stergar and N. J. Cunningham (University of California Santa Barbara), R. J. Kurtz and D. J. Edwards (Pacific Northwest National Laboratory)

OBJECTIVE

Our objective is to experimentally characterize the transport, fate and consequences of high levels of helium in leading candidate fusion alloys.

SUMMARY

The feasibility of fusion energy depends on developing advanced structural materials that can sustain extended component lifetimes in an ultra-severe environment, including up to 200 displacements per atom (dpa) and 2000 appm He. Helium and displacement defects individually and synergistically drive complex microstructural evolutions that degrade many performance-sustaining properties. Managing helium is perhaps the greatest challenge facing fusion structural materials. Here we show that an in situ helium injection fission reactor irradiation at 500°C to ≈ 25 dpa and 1450 appm helium produced populations of both bubbles and growing voids in a leading candidate tempered martensitic steel Eurofer97. The voids, which would be absent at low helium contents, are precursors to rapid swelling, suggesting that tempered martensitic steels may not tolerate extended service in the fusion environment. In contrast, only an ultrahigh density of tiny bubbles form in a companion nano-dispersion strengthened ferritic alloy, MA957. It is expected that the bubbles will inhibit swelling and other deleterious manifestations of irradiation effects at much higher dpa in materials with a high density of stable nano-dispersoids.

INTRODUCTION AND BACKGROUND

Fusion reactors will operate at high temperatures, under intense high-energy neutron fields and large time varying stresses, while exposed to chemically aggressive coolants [1]. High energy neutrons create excess vacancy and self-interstitial atom (SIA) defects by ejecting atoms from lattice sites, generating up to 200 displacements-per-atom (dpa), as well as up to 2000 appm He produced by neutron induced (n,a)) reactions [1-4]. Helium and dpa both individually and synergistically degrade a host of performance sustaining properties. For example, in leading candidate normalized and tempered 9Cr martensitic steels (TMS), grain boundary weakening by helium synergistically interacts with irradiation hardening to produce enormous elevations of the ductile to brittle transition temperature [5-7]. High helium contents may also degrade creep rupture properties at high temperatures and promote void swelling at intermediate temperatures [2-4,8]. Thus managing large quantities of helium is a grand challenge to achieving fusion energy.

Insoluble helium precipitates to form bubbles at elevated temperatures. Bubbles differ from growing voids in that they are smaller, gas pressure-stabilized cavities, containing m helium atoms, which grow only with the addition helium (m -> m+1). Bubble growth occurs up to a critical concentration, m = m*, where they convert to growing voids [2-4]. Larger voids grow by continuously collecting excess vacancies due to the preferential annihilation of the SIA (anti-) defects at biased dislocation sinks. TMS are swelling

resistant in a fission reactor environment where little helium is produced, but accumulating evidence suggests that at high He/dpa ratios growing voids nucleate from helium bubbles at m > m* [2-5]. However, if the bubble number density is very high, then m << m* in any individual bubble. Bubbles are also ideal point defect sinks and deeply trap additional helium that is generated at higher dpa. In this case m* increases and the swelling rate, if voids do manage to form, decreases with increasing bubble number density (N_b) [2-4].

Managing helium by creating a large number of small bubbles is a major objective of the development of an extremely promising alloy class that we call nanostructured ferritic alloys (NFA). NFA contain an ultrahigh density of 2-5 nm diameter Y-Ti-O oxides that are remarkably stable under thermal and irradiation exposure [2,3,9,10]. In addition to promoting high tensile, creep and fatigue strengths [2,3], the nano-dispersed oxides may enhance SIA-vacancy recombination and, most importantly, sequester helium by promoting the formation of a high number density of small, harmless bubbles with m << m*, thus mitigating void swelling [2-4,11]. Such a high matrix bubble sink strength also reduces the amount of helium reaching grain boundaries, thus reducing toughness loss at low-to-intermediate temperatures and potential degradation of creep rupture properties at high temperature [2-4]. Indeed, we have argued that a properly managed high density of nm-scale bubbles could turn helium from a liability to an asset [3].

Fission reactor irradiations normally produce << 1 appm He/dpa. Here we use a novel in situ helium injection (ISHI) technique in mixed spectrum fission reactor irradiations to study the effects of high helium contents on the bubble and void microstructures in TMS and NFA at fusion relevant dpa rates.

MATERIALS AND METHODS

The alloys characterized in this study include TMS and Eurofer97 [12,13], and a 14Cr ferritic stainless NFA, MA957, which has been the focus of many of our previous studies [2,3,10,11,14,15]. The composition of the 6.25 mm Eurofer97 plate used in this study is: 8.93Cr, 1.08W, 0.49Mn, 0.20V, 0.12C, 0.04Si, 0.021N, < 0.01(P, Cu, Co, Ti, Nb, B), bal. Fe (wt%) [12,13]. The plate was austenitized at 980°C for 27 minutes and air-cooled prior to tempering at 760°C for 90 minutes. As shown the transmission electron microscopy (TEM) micrograph in Fig. 1a, the martensite laths in Eurofer97 contain a high density of dislocations and dislocation cell substructures. Eurofer97 also contains alloy carbides distributed over a large size range.

The INCO MA957 used in this study was in the form of a hot extruded 25 mm diameter round bar [16,17]. The nominal MA957 composition is: 14.0Cr, 0.3Mo, 1.0Ti, 0.25Y_2O_3, bal. Fe (wt%) [14]. The specific processing and consolidation parameters for MA957 are proprietary, but the original patent gives the possible conditions including using powders of between -40 and -80 mesh size for each alloying element plus Y_2O_3; attritor milling for 24 h at 288 rpm using a 20:1 ball to powder mass ratio; and a 6:1 extrusion ratio at 1065°C [16]. MA957 contains a very high number density of ≈ $5.1\pm2\times10^{23}/m^3$ NFs with an average diameter of ≈ 2.8±0.4 nm [19]. The bright field TEM micrograph in Fig. 1b shows particularly clear images of the polyhedral oxides down to very small ≈ 1-2 nm sizes in a friction stir welded and annealed condition (FSW-A); note FSW and annealing does not significantly change the number density or the average size and size distribution of the oxides relative to the baseline, as-extruded condition [15,18]. The oxides in the size range < 5 nm are mainly cubic $Y_2Ti_2O_7$ pyrochlore complex oxides

[15]. Figure 1c shows a high resolution TEM micrograph of a $Y_2Ti_2O_7$ particle. MA957 also contains fine ≈ 0.5x5 μm ferrite grains, a high dislocation density and a variety of coarser scale precipitates.

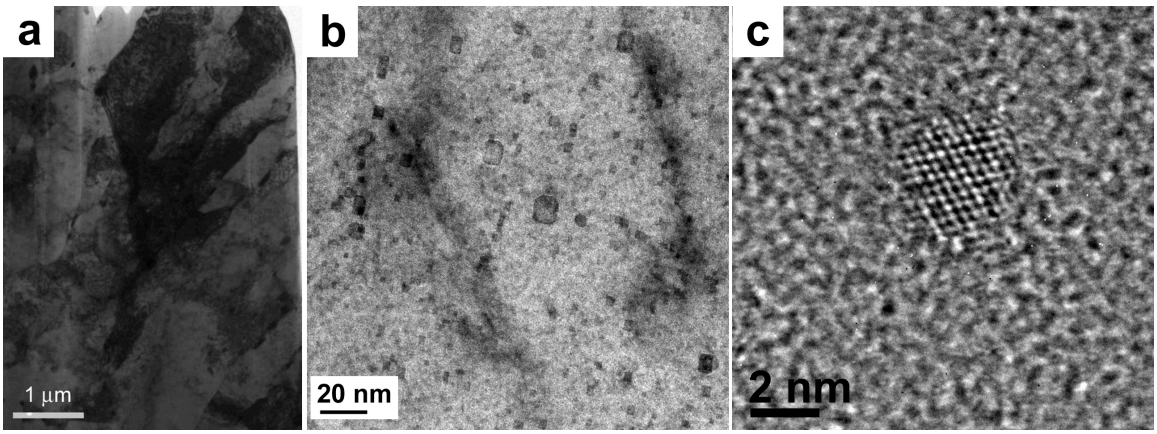

Figure 1. a) Micrograph showing the high dislocation density and lath structure in Eurofer97; b) bright field in foil micrograph showing NF oxides in friction stirred welded and annealed MA957; and, c) a high resolution TEM image of an extracted NF oxide in MA957.

Helium is generated in fast fission and fusion environments by high energy neutron induced endoergic (n,a) reactions with threshold energies in the range of several MeV [4]. Since the energies of most of the fission neutrons are below the (n,a) threshold energy, reactor irradiations normally result in low concentrations of helium and low He/dpa [4]. In contrast the 14 MeV neutrons produced by the DT fusion reaction produce copious amounts of helium. Thus the development of fusion structural materials will likely require a dedicated high-energy neutron source, like the International Fusion Materials Irradiation Facility (IFMIF), to carry out irradiations at a fusion relevant He/dpa ratio and dpa rate [21]. However, facilities such as IFMIF will not be available for some time. Thus, as illustrated in Fig. 2, in the interim, we have designed and implemented a novel in situ helium implantation (ISHI) technique to produce high and controlled levels of He and He/dpa in mixed spectrum fission reactor irradiations [4,8,22,23]. The ISHI technique takes advantage of the fact that thermal neutrons in mixed spectrum fission reactors can produce helium by exoergic (n_{th},a) reactions in a limited number of isotopes, such as ^{10}B. The cross sections for these thermal neutron reactions are large relative to those for fast neutrons. Thus the basic helium implantation concept is to use an implanter layer containing Ni, Li, B, or a fissionable isotope to inject high-energy a-particles from the (n_{th},a) reactions into an adjacent material of interest that is simultaneously undergoing fast neutron-induced dpa damage. In the case of Ni, the helium is generated by two-step reactions: $^{58}Ni(n_{th},g)^{59}Ni(n_{th},a)$. In this study, we have used a thin NiAl layer to uniformly deposit 4.8 MeV a-particles up to a depth of 5-8 μm in the Fe based alloys, depending on the implanter layer thickness. The He/dpa ratio in the ISHI method can be controlled by varying the injector layer thickness, the concentration of the isotope that undergoes the (n_{th},a) reaction, and the thermal to fast neutron flux ratio [4,8,21,22]. Note ^{59}Ni must be bred from ^{58}Ni; thus for the Oak Ridge National Laboratory High Flux Isotope Reactor (HFIR) thermal to fast flux ratio, the helium generated in pure Ni increases from < 1 appm He/dpa, at very low

fluence, to a very broad maximum of ≈ 520 appm He/dpa aound 40 dpa. In this study, ≈ 1 to 4 μm NiAl implanter layers were electron beam deposited on TEM foils and extensively characterized prior to irradiation [24]. The HFIR ISHI experiments to date include a large matrix of Fe-based alloys covering a wide range of dpa, He/dpa (<1 to >50 appm He/dpa) and irradiation temperatures (300 to 500°C) [24]. The helium contents were estimated based on TEM measurements of the implanter layer thickness and composition.

Here we describe new data on the contrasting cavity distributions observed in the TMS, Eurofer97, and the NFA, MA957, following irradiation at 500°C to a neutron fluence of 25 dpa nominally producing ≈ 1400 to 1500 appm He. This helium content is more than two-thirds of the projected maximum end-of-life concentration expected to accumulate in an aggressive demonstration fusion reactor. Note that the nominal He/dpa ratio in HFIR is ≈ 56 to 60 appm/dpa, which is higher than the ≈ 10 appm/dpa in fusion spectra. The higher He/dpa in this study may decrease the incubation dpa (dpa*) for void formation, and may increase the helium bubble density to some extent relative to fusion conditions. However, the subsequent swelling is controlled primarily by the accumulation of dpa, and not the additional helium or the higher He/dpa ratio.

TEM specimens were prepared by focused ion beam micromachining (FIBing) at a low final current of 5.5 pA and voltage of 2 keV. The cavities were characterized using through-focus sequence imaging. They appear as white regions surrounded by a dark ring in the under-focused condition (typically -500 to -1000 nm) and as dark regions surrounded by white rings in the over-focused condition. Cavities were identified by careful comparative image analysis of the under and over-focused micrographs. Cavities were not observed in un-implanted regions, consistent with the well-known high swelling resistance of Eurofer97 and F82H in the absence of sufficient helium. The absolute diameters of the bubbles cannot be determined precisely, especially at small sizes, without detailed corrections. The cavity diameters reported here are the nominal values for the white spot diameter in the under-focused condition. Foil thicknesses were determined by convergent beam electron diffraction.

RESULTS AND ANALYSIS

We previously reported in situ helium implantation results for irradiations up to ≈ 9 dpa and 380 appm He [8,11]. Here, we first briefly summarize the key results of characterizing the TMS and NFA used in this study. We next describe the results of the in situ helium injection experiment, contrasting the behavior of the TMS and NFA. The bubble size distribution and an equation of state are used to estimate the helium content of the bubbles in MA957. Finally we use simple rate theory concepts to examine and extrapolate the significance of these new results.

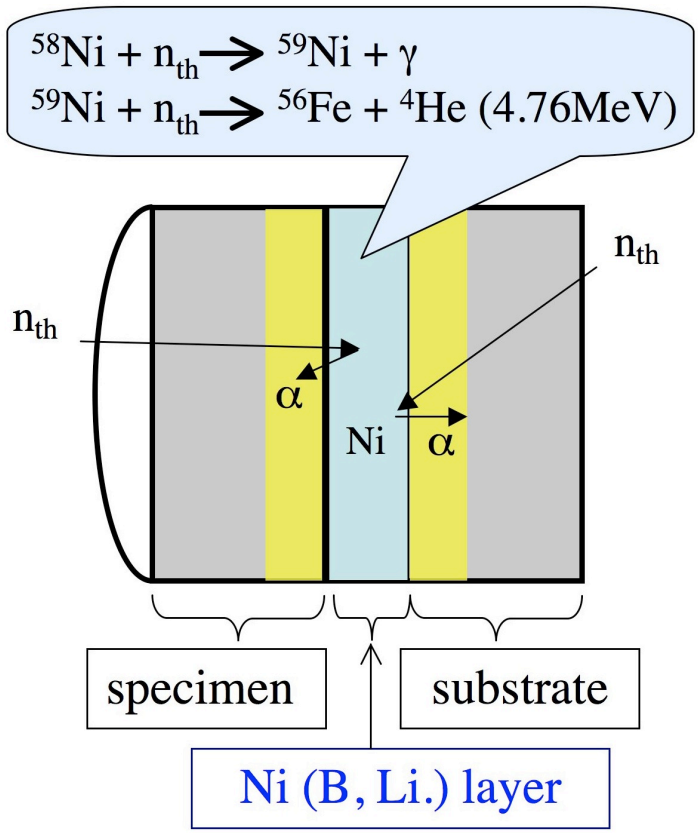

Figure 2. Schematic illustration of the ISHI method.

Figure 3a and b shows a typical example of through focus sequence micrographs for Eurofer97 and Figure 3c and d show the corresponding micrographs for MA957. Figure 4 shows the corresponding cavity size distributions. Clearly, the differences in the cavity size distributions in the two alloys are profound. Eurofer97 contains a bi-modal cavity size distribution, consisting of small bubbles and larger growing voids, with an apparent pinch-off size at d ≈ 2 nm. As previously observed, the voids are polyhedral, with low index facets that minimize the total surface energy. Assuming that the pinch-off marks the critical size, d*= 2r*, the bubbles and voids represent ≈ 52 and 48% of the total of ≈ $7.5 \times 10^{22}/m^3$ cavities in Eurofer97, respectively. The corresponding average diameters, <d>, are ≈ 1.2 nm (bubbles) and ≈ 5 nm (voids). Helium inventory balances, as described for MA957 below, clearly show that the total helium content in the in situ helium implantation irradiated Eurofer97 is far too low for the larger, <d> = 5 nm cavities to be pressurized bubbles. Comprehensive examinations (not shown) suggest that the bubbles are primarily located on dislocations, or at least at the previous locations of dislocations, as well as on lath boundaries and carbide interfaces. The total swelling in Eurofer97 of about 0.5% is almost all due to the voids.

In contrast, there is a much higher density of helium bubbles, ≈ $7.8 \times 10^{23}/m^3$, in the NFA MA957 with <d> ≈ 1.3 nm, and no voids. The bubbles are uniformly distributed

throughout the matrix In this case, presumably in association with small oxides. Other bubbles are more clearly visible on the interfaces of larger precipitates.

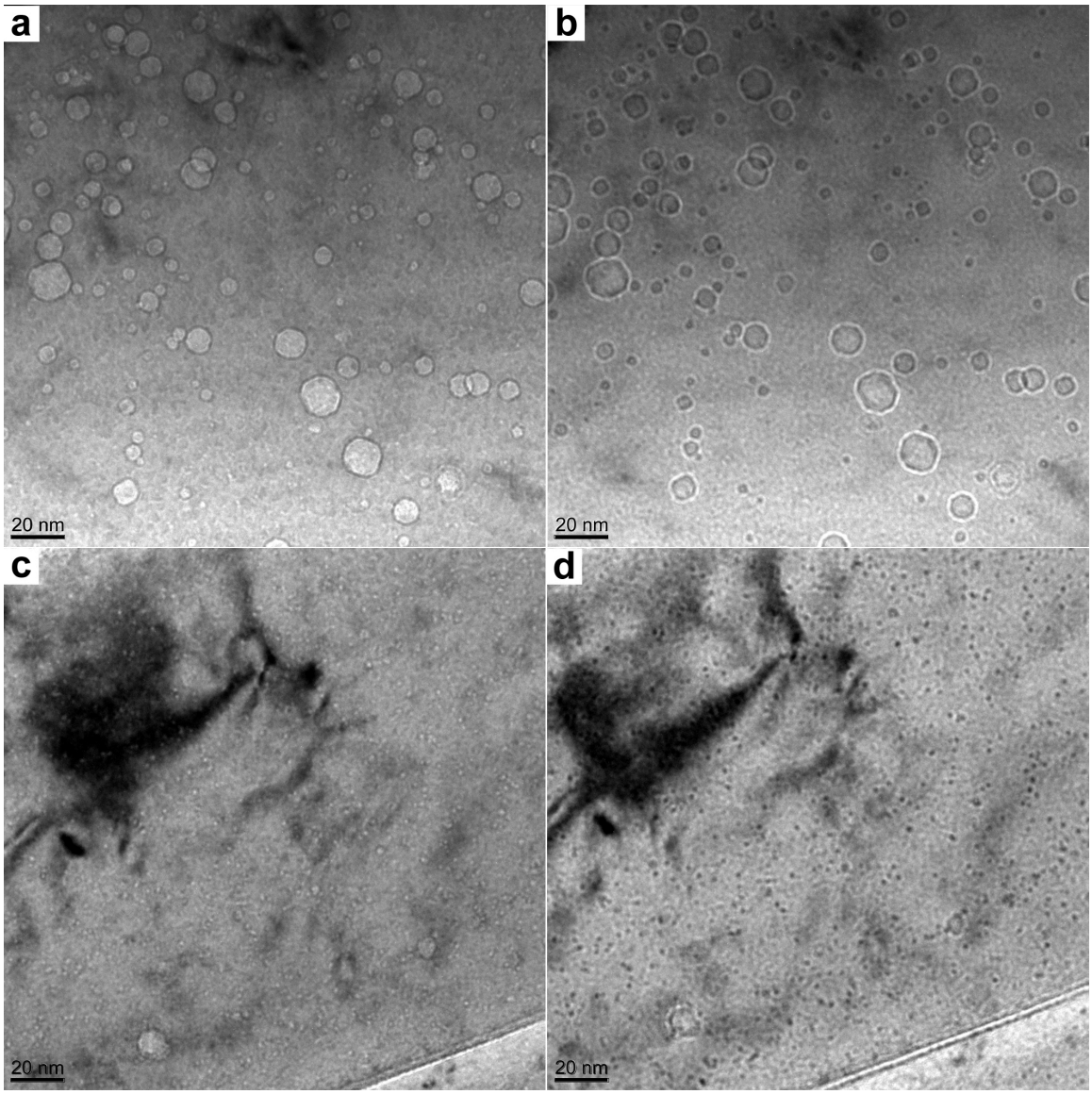

Figure 3. a and b) Under- and over-focused images of cavities in Eurofer97; c and d) under- and over-focused images of cavities in MA597.

It is useful to estimate the helium content of the bubbles in MA957. Assuming the simple capillary approximation for the helium gas pressure [25], p, is

$$p \approx 2g/r_b \approx [3zmkT]/[4\pi r_b^3]. \qquad [1]$$

Here g is the surface energy and z(p) is the helium compressibility factor. The concentration of helium atoms in the bubbles can be estimated as

$$He_{tb} \approx [8\pi g/3N_a kT]_{S_i}[N_{bi} r_i^2/z(r_i)]. \quad [2]$$

The r_i and N_{bi} are the nominal radius of the i'th bubble size and number density, respectively; N_a is the number of atoms/m^3. Taking g = 2.5 J/m^2 and determining z(p) from a hard sphere high pressure equation of state [25], the estimated $He_{tb} \approx 1170$ appm, in reasonable qualitative agreement with the nominal total estimated helium content. However, this estimate is subject to various uncertainties. Briefly, the bubbles may be somewhat smaller than the nominal size determined in the under-focused condition [26,27], and the continuum equation of state may overestimate the He/V ratio and the He_{tb} in small bubbles [28]. However, as shown in Figure 5, the predicted helium density (He/nm^3) is in fair agreement with measurements obtained from electron energy loss spectroscopy (EELS) at small bubble sizes [29]. Further, lower values of g and contributions from invisible bubbles would lead to higher estimates of He_{tb}. Note, thermodynamic and kinetic considerations suggest that it is unlikely that a significant amount of helium remains in solution at 500°C.

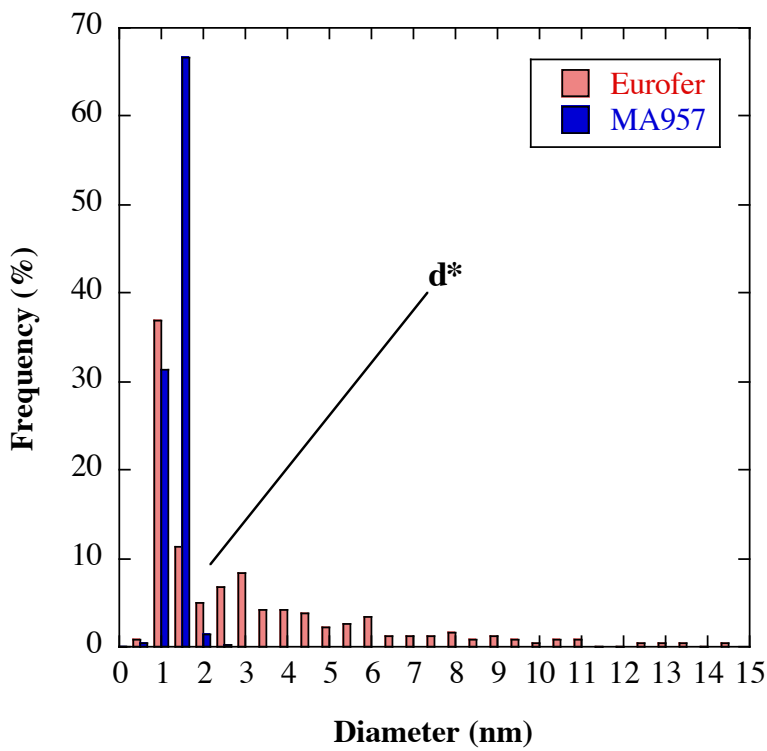

Figure 4. Comparison of the size distributions in Eurofer97 and MA957 irradiated to similar dpa and helium concentrations.

A simplified form of rate theory was used to assess the swelling resistance of the NFA based on scaling arguments, rather than a detailed numerical assessment [4]. In this framework, the effective vacancy super-saturation, L > 1, is the ratio of the net vacancy flux (vacancies minus SIA) at unbiased (neutral) sinks to the corresponding thermal vacancy flux in the absence of irradiation, where the latter is controlled by the self-diffusion coefficient, D_{sd}: $L = (D_vX_v - D_iX_i)/D_{sd}$. The critical helium content m* scales with $1/[\ln(L)]^2$. Hence for small L-1, m* scales as $1/[L-1]^2$. In the simplest case prior to the conversion of bubbles to voids, and neglecting other sinks, L-1 can be expressed in terms of the sink strengths for bubbles and dislocations, Z_b and Z_d, respectively, and a bias factor of dislocations for SIA (B). For B << 1, L-1 scales with $Z_d/[Z_b+Z_d]^2$. The sink strength for 7.5×10^{22}, 1.2 nm bubbles in Eurofer97 is $Z_b \approx 5.6\times10^{14}/m^2$ and $Z_b \approx 6.4\times10^{15}/m^2$ for the 7.8×10^{23}, 1.3 nm bubbles in MA957. A reasonable nominal value for the dislocation sink density is $Z_{rd} \approx 5\times10^{14}/m^2$ in both cases. Based on these values, m*[MA957]/m*[Eurofer97] ≈ 900. Since the helium is divided into ≈ 10 times more bubbles in MA957 compared to Eurofer97, the corresponding ratio of the incubation dpa, dpa*[MA957]/dpa*[Eurofer97], needed to form a significant population of voids would be even larger.

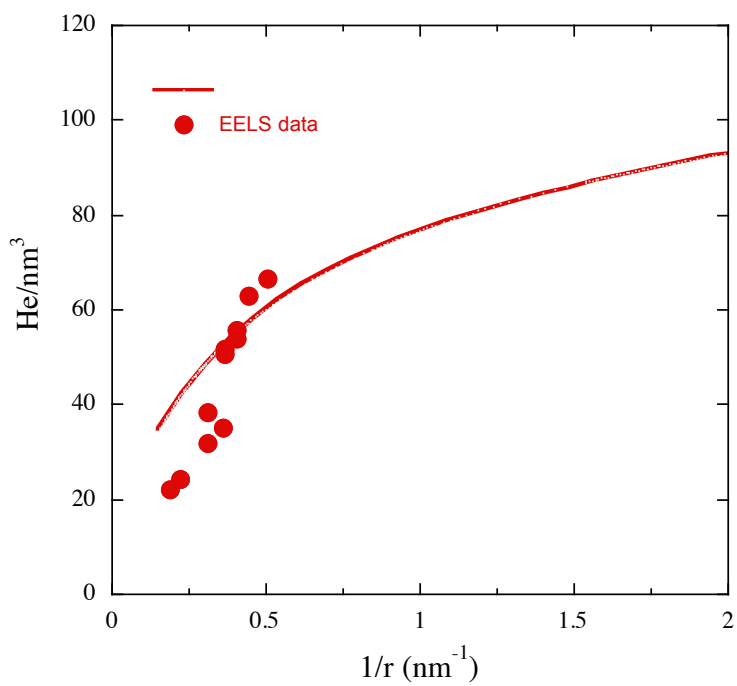

Figure 5. The EOS helium density compared to EELS measurements reported in the literature [29].

While the numerical values derived from these simple rate theory based scaling assessments should not be taken too seriously, they illustrate that persistent swelling resistance associated with a large population of small bubbles in NFA is to be expected. The critical bubble model and simple rate theory concepts can also be used to

approximately extrapolate these results to higher helium and dpa. Assuming no new bubbles are formed in MA957, then 2000 appm helium would increase the average bubble diameter from the nominal average of ≈ 1.3 to ≈ 1.5 nm, which is still well below the estimated r* and m* for the high bubble sink density in MA957. Note that in principle, the defect fluxes driving other irradiation effects are also reduced with increasing total sink strength; and the fraction of helium reaching grain boundaries would be likewise diminished at high bubble densities.

The prognosis for TMS swelling resistance at higher helium and dpa levels is much less promising. Higher helium would convert more bubbles to voids. A void (converted from bubbles) to dislocation sink strength ratio that is close to being balanced (≈ 0.5 to 2) would lead to an approximately maximum swelling rate [2,4]. A previous ISHI irradiation at 500°C of TMS F82H showed that voids begin to form at ≈ 200-400 appm He (9), and the results reported here further show they are the dominant sink at ≈ 1500 appm He. Once formed, the voids continue to grow with increasing dpa. Notably, helium plays a much smaller role in the post-incubation swelling regime. Garner has argued that the steady state swelling rate in bcc steels is about 0.2%/dpa [30]. Assuming this swelling rate, and that for fusion relevant conditions a large population of voids form by 1000 appm He and 100 dpa, then at 200 dpa the total swelling in TMS would reach a clearly intolerable level of more than 20%. Practical swelling limits would probably be much lower.

Thus this work leads two very important *proof of principle* conclusions: a) the helium rich fusion environment will limit extended service of TMS alloys at intermediate temperatures; and, b) NFA can manage helium and manifest persistent damage resistance, greatly extending the potential lifetimes of fusion structures.

SUMMARY AND CONCLUSIONS

The helium content in the present HFIR in situ helium implantation experiment is more than two-thirds of the end-of-life levels projected for fusion first wall and blanket structures. Key conclusions from this study include:

- The in situ helium implantation method provides a powerful new tool for characterizing the effects of He-dpa synergisms on microstructural evolutions in virtually any material.
- High helium contents promote the formation of a large population of voids in TMS that would be largely absent at lower helium and He/dpa levels.
- Essentially the same amount of helium is sequestered in a very high density of nm-scale bubbles in NFA, with no voids present.
- Simple rate theory scaling extrapolations suggest that NFA will remain irradiation damage tolerant up to much higher dpa and helium levels.
- In contrast, extrapolations for TMS suggest that the observed voids are precursors to significant void swelling at higher dpa, leading to the conclusion that TMS will not be suitable for service to 200 dpa in fusion first wall structures.

The results reported here will be extended to a much wider range of temperatures, dpa, He/dpa ratios and alloys based on the large existing and future matrix of ISHI irradiation conditions. Detailed models also being developed to assess the transport, fate and

consequences of helium are broadly consistent with the crude estimates of the behavior of NFA and TMS outlined above [31].

Finally, it is important to note that NFA are in a very early stage of development and qualification for fusion, advanced fission and other hostile service applications. However, we believe that their immense promise warrant a major science based research effort.

ACKNOWLEDGMENTS

The US Department of Energy (DOE), Office of Fusion Energy Sciences supported the research described here in contracts DE-FG03-94ER54275 (UCSB) and DE-AC06-76RLO1830 (PNNL). The authors acknowledge the significant contributions of Drs. R. Stoller and D. Hoelzer, as well as many of their Oak Ridge National Laboratory colleagues for their time and effort for the HFIR irradiations and providing the specimens for examination. The TEM specimen preparation was carried out at the Center for Advanced Energy Systems in Idaho Falls, Idaho under the sponsorship of the DOE Idaho National Laboratory ATR National Users Facility. TEM measurements were carried out in the UCSB Materials Research Laboratory Microstructure and Microanalysis Facility, supported by the Materials Research Science and Engineering Center Program of the National Science Foundation under award no. DMR05-20415.

REFERENCES

[1] S. J. Zinkle and J. T. Busby, *Mater Today* (2009)**12**:12.

[2] G. R. Odette, M. J. Alinger, and B. D. Wirth, *Annu. Rev. Mater. Res.* (2008) **38**:471.

[3] G. R. Odette and D. T. Hoelzer, *JOM* (2010) 62:84.

[4] Y. Dai, G. R. Odette, and T. Yamamoto, Comprehensive Nuclear Materials, Chapter 6, "The Effects of Helium in Irradiated Structural Alloys," 2012; in press.

[5] T. Yamamoto, G. R. Odette, M. Salston, P. Miao, and Y. Dai, Trans. Am. Nucl. Soc. *(2008)* ***98****:1111.*

[6] T. Yamamoto, G. R. Odette, H. Kishimoto, J-W. Rensman and P. Miao, *J. Nucl. Mater*. (*2006)* **356**:27.

[7] G. R. Odette, T. Yamamoto, H. J. Rathbun, M. Y. He, M. L. Hribernik, and J. W. Rensman, *J. Nucl. Mater. (2003)* **323**:313.

[8] T. Yamamoto, G. R. Odette, P. Miao, et al., *J. Nucl. Mat*. (2009) **386:**338.

[9] M. K. Miller, D. T. Hoelzer, E. A. Kenik, and K. F. Russell, *J. Nucl. Mater.* (2004) **329**:338.

[10] N. J. Cunningham, et al., "Long-Term Thermal Aging Effects on the Microstructure of Ferritic Alloy MA957," in preparation.

[11] G. R. Odette, P. Miao, D. J. Edwards, et al., *J. Nucl. Mater.* (2011) **417**:1001.

[12] R. J. Kurtz, A. Alamo, E. Lucon, et al., *J. Nucl. Mater.* (2009) **386**:411.

[13] H. E. Hofmans, NRG Report 20023/00.38153/P, 2000, Petten, The Netherlands.

[14] M. J. Alinger, G. R. Odette and D. T. Hoelzer, *Acta Mater.* (2009) **57**:392.

[15] Y. Wu, E. Haney, N. Cunningham and G. R. Odette, "Transmission Electron Microscopy Characterization of the Nanofeatures in Nanostructured Ferritic Alloy MA957," submitted to *Acta Mater*. (2011) under review.

[16] J. J. Fisher, U.S. Patent No. 4,075,010, 1978.

[17] H. L. Hamilton, D. S. Gelles, R. J. Lobsinger, G. D. Johnson, W. F. Brown, M. M. Paxton, R. J. Puigh, C. R. Eiholzer, C. Martinez, and M. A. Blotter, Technical Report, PNL-13168, 1991.

[18] A. Etienne, N. J. Cunningham, Y. Wu, et al., *Mat. Sci. Tech*. (2011) **27-4**:724.

[19] N. J. Cunningham, G. R. Odette, E. Stergar et al., DOE Fusion Materials Semiannual Progress Report, June 30, 2011; DOE/ER-0313/50: in press.

[20] D. T. Hoelzer, J. P. Shingledecker, R. L. Klueh et al., Fusion Materials Semiannual Report 6/30/2010 2011; DOE/ER-313/48:50.

[21] P. Garin and M. Sugimoto, *Fusion Eng. Des.* (2008) **83**:971.

[22] G. R. Odette, *J. Nucl. Mater.* (1986) **141**:101.

[23] L. K. Mansur and W. A. Coghlan, **"**Effects of Radiation on Materials": 14th International Symposium 1989 ASTM STP 1046; 2:315.

[24] T. Yamamoto, G. R. Odette, and L. R. Greenwood, Fusion Materials Semiannual Report 6/30/2005 2005; DOE/ER-313/38:95.

[25] R. E. Stoller and G. R. Odette, *J. Nucl. Mater.* (1985) **131**:118.

[26] M. Ruhle and M. Wilkens, *Cryst. Latt. Defects* (1975) **6**:129.

[27] X. Zhang, E. G. Fu, A. Misra, and M. J. Demkowicz**,** *JOM* (2010) **62-12**:75

[28] D. Stewart, Y. Osetskiy, and R. E. Stoller, *J. Nucl. Mater*. (2011) **417**:1110.

[29] S. Fréchard, M. Kociak, M. Walls, J. P. Chevalier, J. Henry, and D. Gorse, *J. Nucl. Mater.* (2009) **393**:102.

[30] F. A. Garner, M. B. Toloczko, and B. H. Sencer, *J. Nucl. Mater.* (2000) **276**:123.

[31] T. Yamamoto, G. R. Odette, R. J. Kurtz, and B. D. Wirth, Fusion Materials Semiannual Report 12/31/2010 2011; DOE/ER-313/49:73.